Electronic Supplementary Material (ESI) for Soft Matter.

Supplementary Materials: Magnetophoresis of Paramagnetic Metal Ions in Porous Media

Peter Rassolov,[1,2] Jamel Ali,[1,2] Theo Siegrist,[1,2] Munir Humayun,[2,3] and Hadi Mohammadigoushki[1,2]

[1)] *Department of Chemical and Biomedical Engineering, FAMU-FSU College of Engineering, Florida State University, Tallahassee, FL, 32310, USA*

[2)] *National High Magnetic Field Laboratory, Tallahassee, FL, 32310, USA*

[3)] *Department of Earth, Ocean and Atmospheric Science, Florida State University, Tallahassee, FL 32304, USA.*

(Dated: 9 February 2024)

I. ESTIMATION OF THE DEBYE LENGTH

The metal salts used by Fujiwara et al. and modeled in this study consist of metal cations and chloride anions, and the driving forces for fluxes of the cations may differ from those of the anions. In particular, any electric fields that may be externally applied or induced by motion of the ions can give rise to electric migration. However, local electroneutrality can be assumed if all relevant length scales are larger than the Debye length of the solution studied. The Debye length λ is given by the Debye-Huckel approximation[1]:

$$\lambda = \left(\frac{F^2}{\varepsilon_r \varepsilon_0 RT} \sum_i z_i^2 C_i \right)^{-1/2}, \tag{1}$$

where F is the Faraday constant (96485 C/mol), ε_r is the dielectric constant (79.5), ε_0 is the vacuum permittivity (8.854 $\times 10^{-12}$ F/m), R is the molar gas constant (8.314 J/mol·K), T is the temperature (295 K), z_i is the charge of species i, and C_i is the concentration of species i. For this study, the concentration of the solute species varies in space and time; accordingly, the Debye length varies as well, with lesser concentrations giving rise to longer Debye lengths. A reasonable lower limit for the detectable concentration is 10^{-4} M, or 0.01 % of c_0. Therefore, $\lambda \leq 16$ nm for the conditions in this study; selected possible values for λ are given in Table S1. This is several orders of magnitude less than the smallest resolved feature in the continuum based simulations of this study; the initial diameter of the ion spot. Additionally, the solute is a binary electrolyte that does not undergo reactions or boundary fluxes; therefore, for this study, the solute is modeled as a single neutral species that does not undergo migration driven by electric fields.

TABLE S1. Debye lengths for the salts used in this study in a range of detectable concentrations.

Cation valence	+2	+3
c [M]	λ [nm]	
1	0.16	0.12
0.1	0.51	0.38
0.01	1.6	1.2
10^{-3}	5.1	3.8
10^{-4}	16	12

II. THREE-DIMENSIONAL MODELING

The simulations reported in this study represent the magnet and silica gel channel in the plane normal to the narrowest channel dimension (the depth) using 2D Cartesian coordinates. While this is an accurate representation of the channel, it is necessarily an approximation of the superconducting magnet coil and the resulting magnetic field. For an exact representation of the coil and channel geometry, a full 3D model is needed. To conduct the full study reported in this work in 3D space would have a prohibitive computational cost.

Nonetheless, a comparison of planar 2D with 3D simulations is needed to verify that the 2D magnetic field is a valid approximation. Here, we report one such 3D study.

The computational porous medium domain used the same 40 mm width × 140 mm length as the 2D models, while the thickness was 5 mm, consistent with Fujiwara et al. To match the 2D simulations, this domain was filled with tetrahedral mesh elements each 0.33 mm in size, for a total of 13,008,583 elements in which the full set of electromagnetic and species transport equations were solved. The coil mesh was constructed by creating 6 mm triangular elements through its radial cross section; this 2D mesh was revolved to construct a 3D mesh of 23,904 triangular prism elements. Outside the magnetophoresis channel and coil, the mesh elements gradually increased in size with distance from the channel and coil. The overall magnetic field domain was a sphere of radius 5 m filled with 15,175,318 elements. The coil inner diameter was increased to 102 mm, the length was increased to 162 mm, and the turns × current was reduced to 1.33 MA to maintain the best possible match of the simulated magnetic field to data reported by Fujiwara et al.[2]. The arrangement of the porous medium domain and the coil are illustrated in Fig. S1.

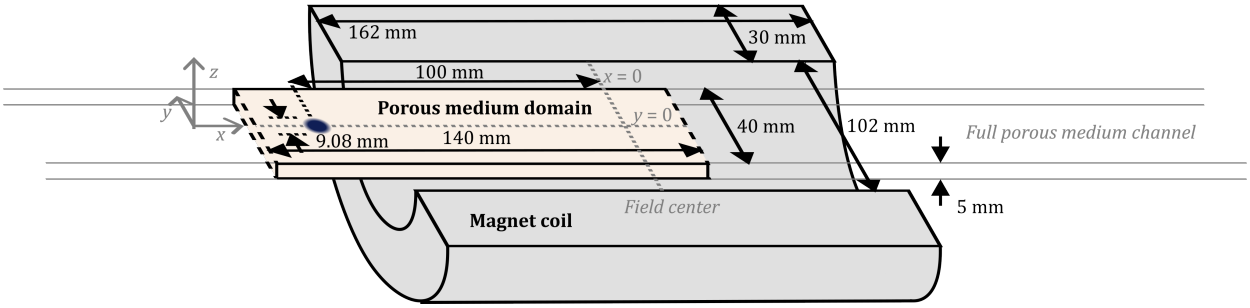

FIG. S1. Cut-away view of the domains used for 3D simulations showing dimensions of the coil and the computational domain that contains the porous medium. The dimensions of the magnet are as follows: inner radius of the magnet coil 51 mm, outer radius 81 mm, length 162 mm, number of turns × current 1.33 MA.

.

Figure S2 summarizes the magnetic field and temporal evolution of a spot of copper (II) ions under the same conditions as Fig. 4 in the main text. Overall, the magnetic field best matching Fujiwara et al. is concentrated within the magnet bore, and the spanwise component of $(\mathbf{B} \cdot \nabla)\mathbf{B}$ is slightly less compared to the best matching 2D magnetic field. Nonetheless, these differences in the magnetic field are minimal at the center line of the porous medium domain, where the spot of ions is centered and where further analysis is conducted. Indeed, the evolution of the peak shape shown in subfigure (d) and peak height and location in subfigure (e) show good agreement with Fig. 4(e) in the main text and with the prior experimental data. Therefore, meaningful conclusions can be drawn from the 2D planar simulations. On the other hand, the 3D simulation required approximately 6 hours of computing time, while the equivalent 2D simulation required only 15 minutes on the same hardware. Therefore, the computational cost of each 3D simulation is the major drawback. Since the results reported in this study are based on about 100 simulations, repeating all simulations in 3D would require about 600 hours of computing time without producing significant new insights. Therefore, we decided to keep and present the 2D simulation results in the manuscript.

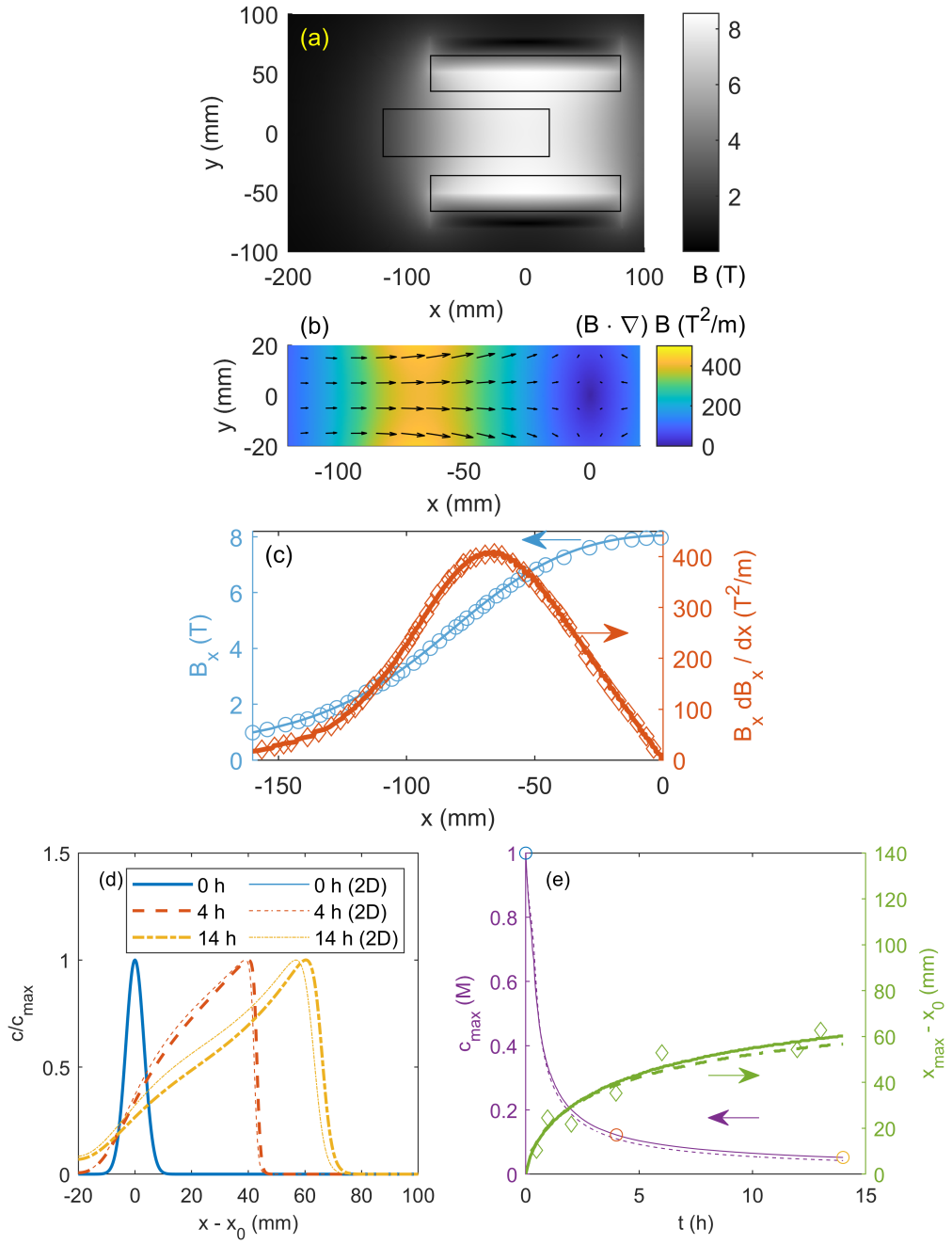

FIG. S2. (a) Map of the magnetic flux density in a cross-section of the 3D domain. (b) Map of the magnetic field gradients ($(\mathbf{B}\cdot\nabla)\mathbf{B}$) in the porous medium domain. (c) Magnetic flux density and the gradients along the magnet center line shown for both experiments and 3D simulations. Reprinted (adapted) with permission from Fujiwara et al.[2]. Copyright 2001 American Chemical Society. (d) Normalized center line concentration profiles following 0, 4, and 14 h of exposure to the magnetic field. Predictions from 2D simulations are shown as narrower lines. (e) Temporal evolution of the spot location and maximum spot concentration. The solid lines are predictions of 3D simulations, and the dashed lines are the predictions from 2D. Circular markers show the times plotted in subfigure (d), and diamond-shaped markers are experimental results reported in Fujiwara et al.[3]. Reprinted (adapted) with permission from Fujiwara et al.[3]. Copyright 2006 American Chemical Society.

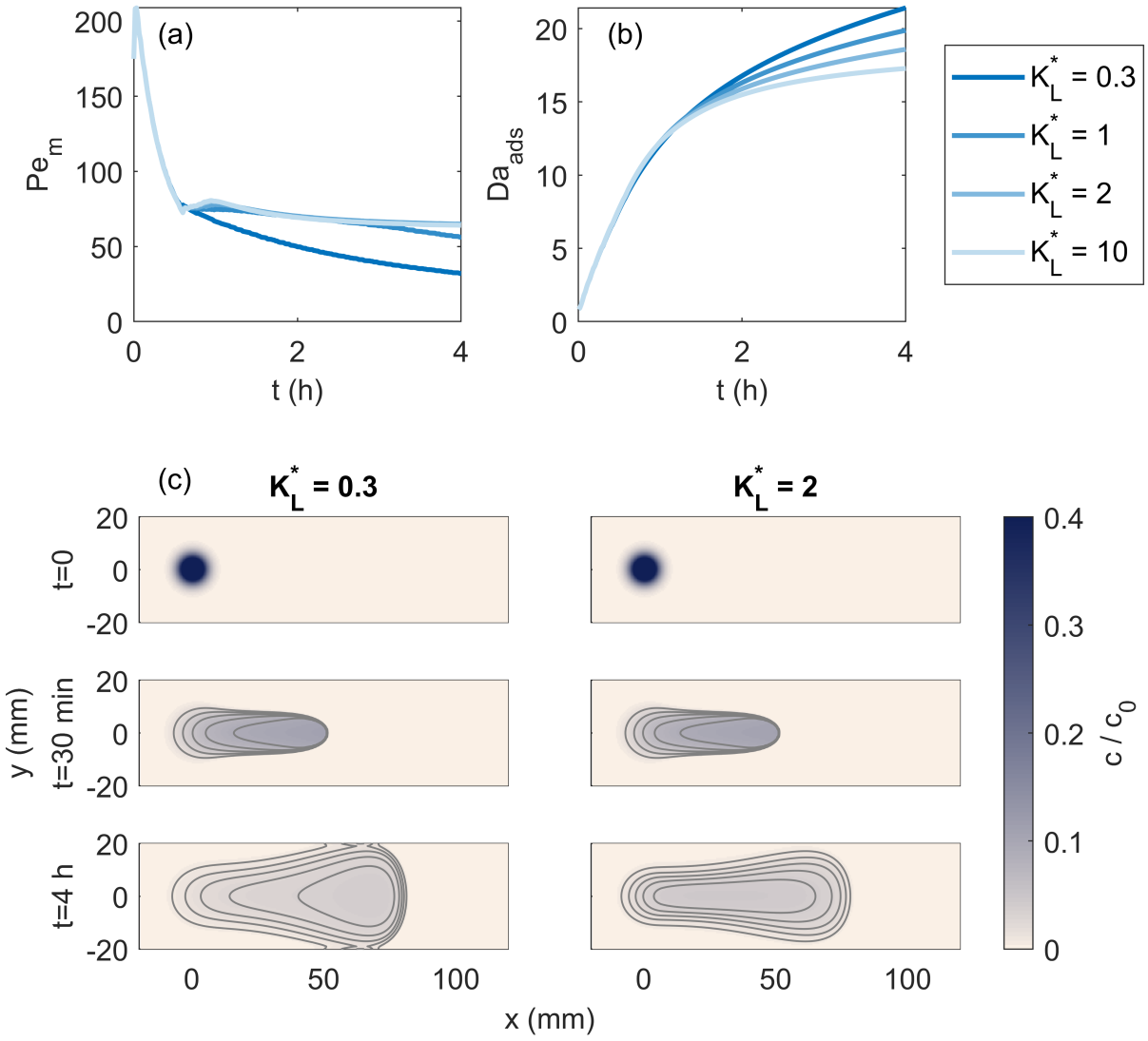

FIG. S3. Effect of the Langmuir adsorption coefficient K_L^* on magnetomigration of iron (III) chloride. Temporal evolution of the magnetic Péclet number (a) and the adsorption Damkohler number (b). (c) A series of images illustrating the spatio-temporal evolution of iron (III) chloride ion concentration distribution at selected times for $K_L^* = 0.3$ and 2.

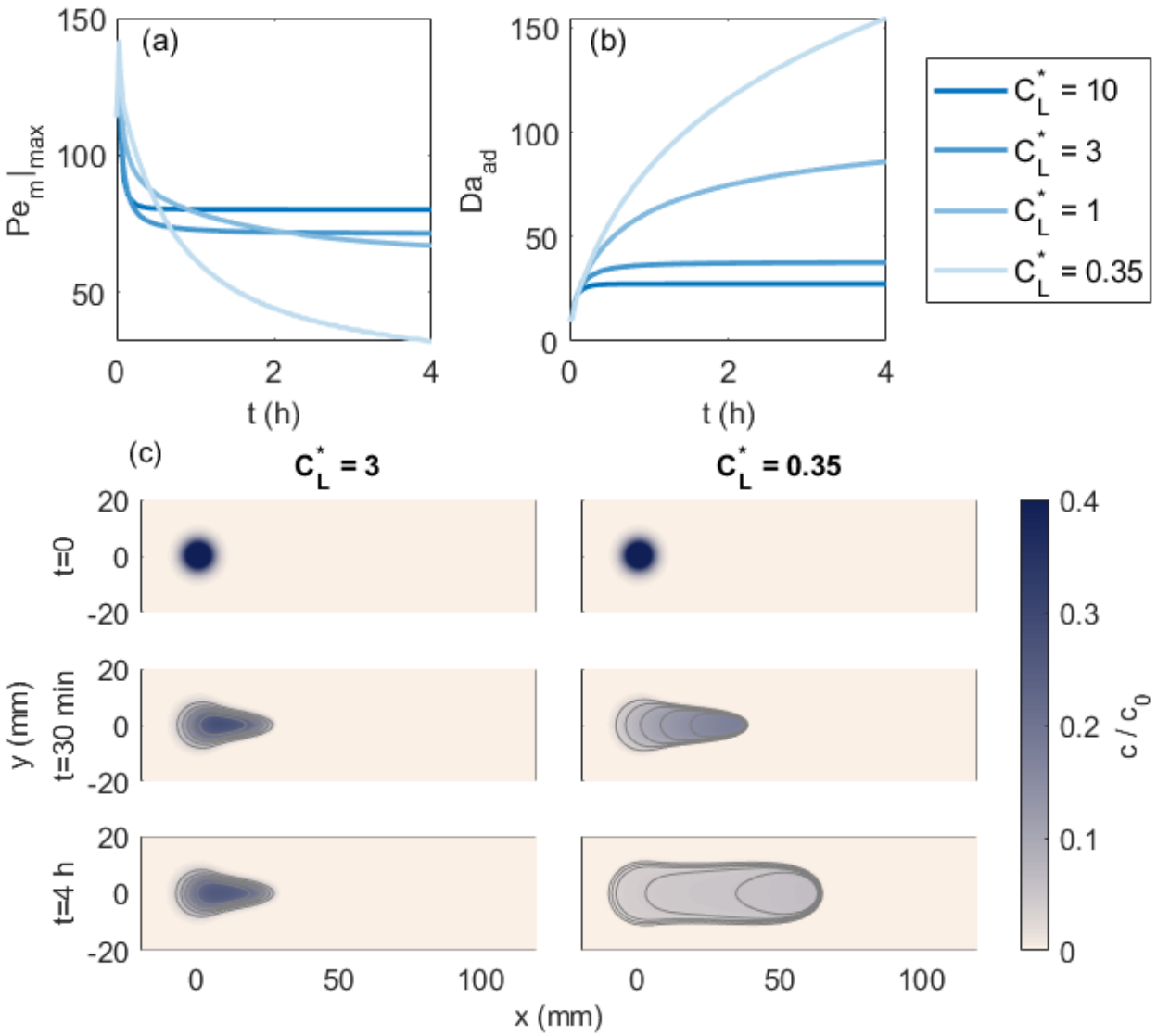

FIG. S4. Effect of the maximum adsorbed concentration C_L^* on magnetomigration of cobalt (II) chloride. Temporal evolution of the magnetic Péclet number (a) and the adsorption Damkohler number (b). (c) A series of images illustrating the spatio-temporal evolution of cobalt (II) chloride ion concentration distribution at selected times for $C_L^* = 3$ and 0.35.

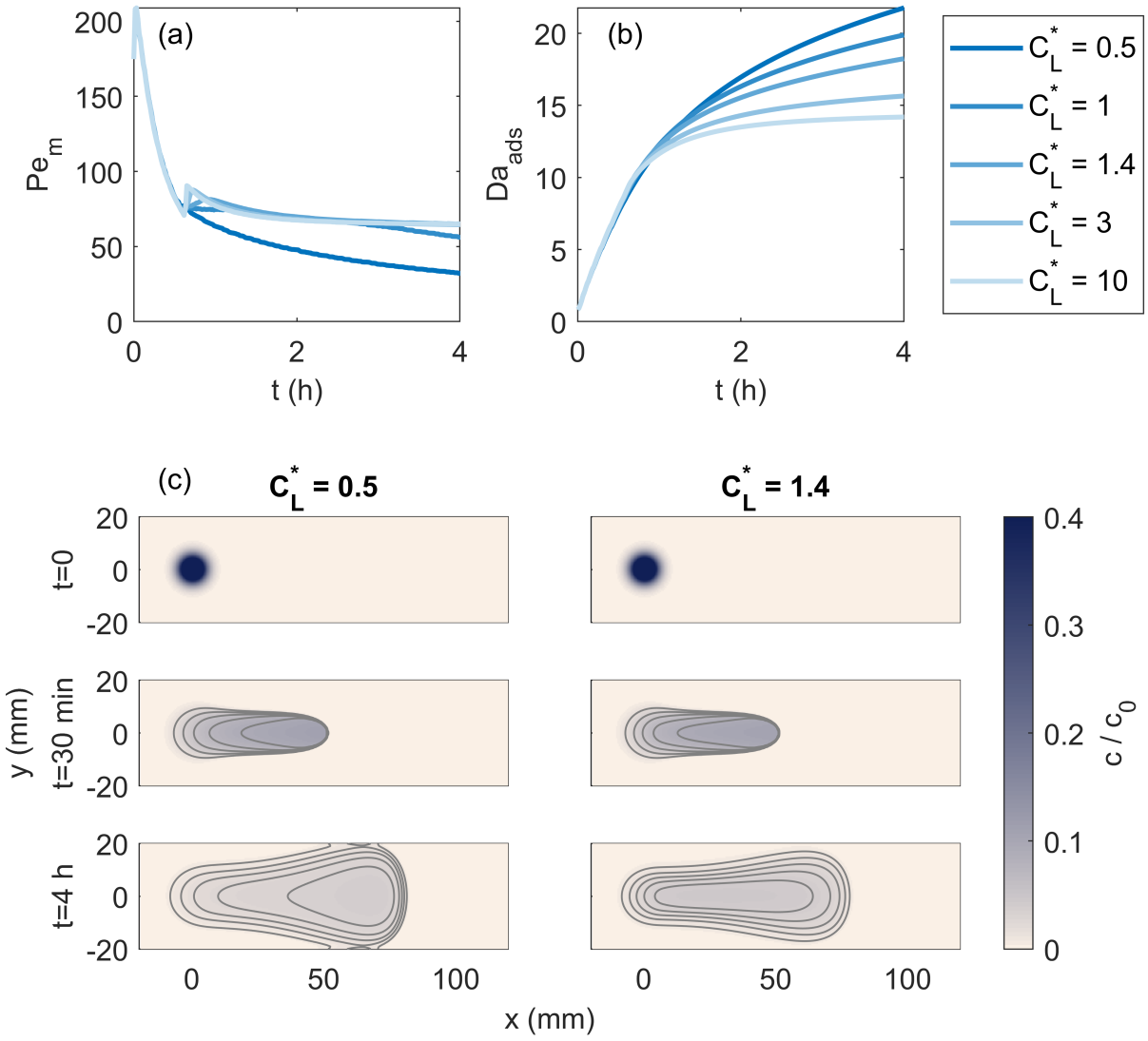

FIG. S5. Effect of the maximum adsorbed concentration C_L^* on magnetomigration of iron (III) chloride. Temporal evolution of the magnetic Péclet number (a) and the adsorption Damkohler number (b). (c) A series of images illustrating the spatio-temporal evolution of iron (III) chloride ion concentration distribution at selected times for $C_L^* = 0.5$ and 1.4.

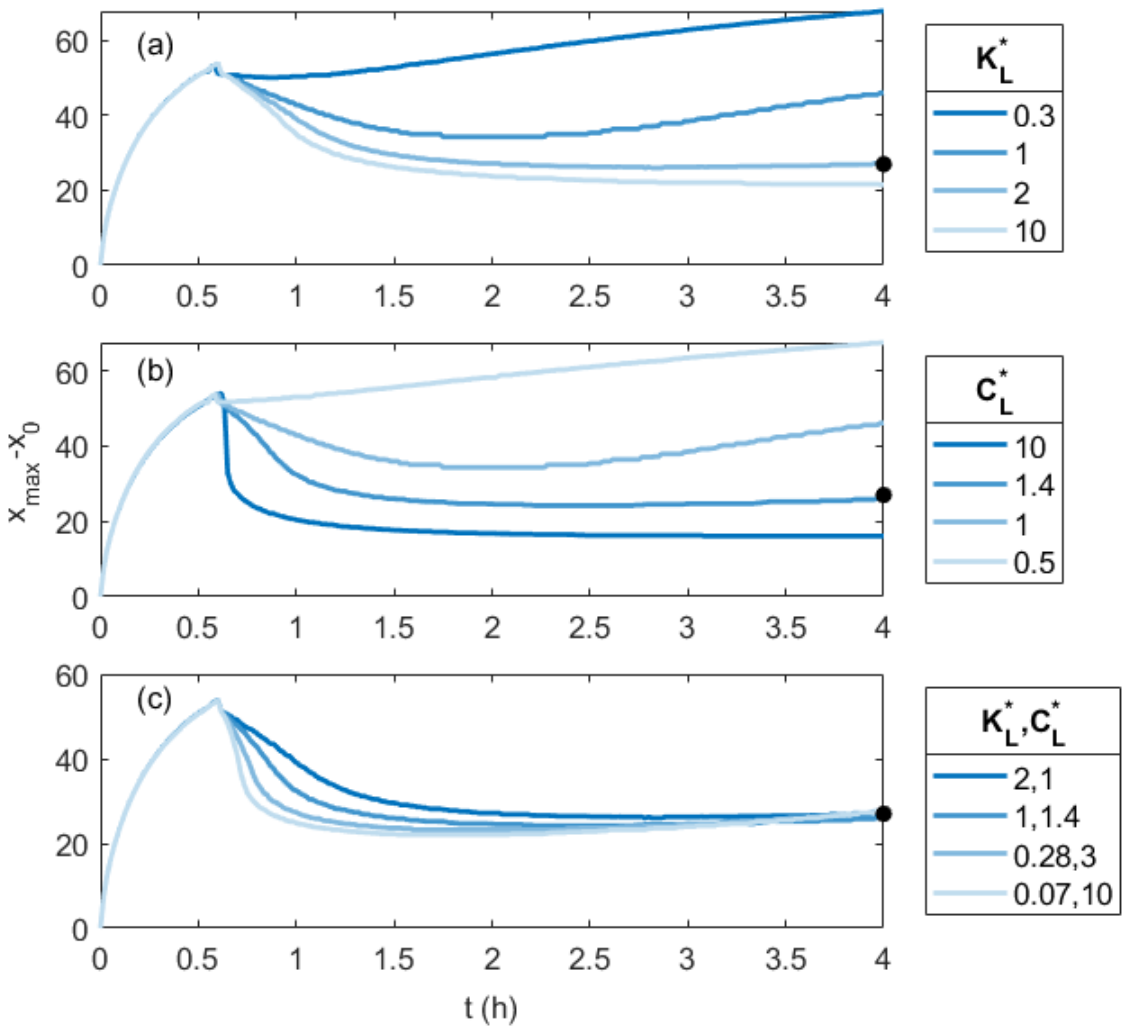

FIG. S6. Predicted movement of the spot of iron (III) chloride for varied adsorption parameters. (a) Effect of the Langmuir adsorption coefficient K_L^* (b) and adsorption saturation concentration C_L^* (b) on the movement of the concentration maximum. For this study, the product $k_{ad}C_L$ was held fixed. (c) Movement of the point of maximum concentration for various (K_L^*,C_L^*) pairs resulting in the same movement after 4 h. The black dots in (a-c) denote the experimental results of Chie et al.[4].

REFERENCES

[1]William M Deen. *Analysis of Transport Phenomena*. Oxford University Press, second edition, 2012.

[2]M Fujiwara, D Kodoi, W Duan, and Y Tanimoto. Separation of transition metal ions in an inhomogeneous magnetic field. *The Journal of Physical Chemistry B*, 105(17):3343–3345, 2001.

[3]M Fujiwara, K Mitsuda, and Y Tanimoto. Movement and diffusion of paramagnetic ions in a magnetic field. *The journal of physical chemistry B*, 110(28):13965–13969, 2006.

[4]K Chie, M Fujiwara, Y Fujiwara, and Y Tanimoto. Magnetic separation of metal ions. *The Journal of Physical Chemistry B*, 107(51):14374–14377, 2003.